Engineering Failure Analysis 152 (2023) 107430

Contents lists available at ScienceDirect

Engineering Failure Analysis

journal homepage: www.elsevier.com/locate/engfailanal

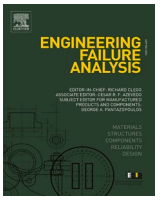

A numerical insight into the reliability of seismic strength models for masonry piers and spandrels

Michele Betti [a,*], Luciano Galano [a], Francisco J. Pallarés [b]

[a] Department of Civil and Environmental Engineering, University of Florence, Via S. Marta 3, 50139 Florence, Italy
[b] ICITECH, Universitat Politècnica de València, amino de Vera s/n, 46022 Valencia, Spain

ARTICLE INFO

Keywords:
Brick
Masonry
Seismic analysis
FE analysis
Failure analysis
Piers
Spandrels
Strength models

ABSTRACT

With the aim to provide an insight on the effectiveness of existing formulae for the flexural and shear strength of masonry piers and spandrels, this paper reports and compares results obtained from pushover analyses performed on a set of plane masonry walls. As reference, the formulae provided by the Italian Building Code (IBC) were considered. Nonetheless, the formulations provided by IBC are similar to the ones reported in the Eurocode Standards (ES), and thus conclusions of this paper can be extended to the latter. Three types of masonry walls were considered which differ in the span-to-height ratio b/h of the masonry beams, namely: a) slender beams ($b/h = 2.0$); b) intermediate beams ($b/h = 1.00$) and c) short beams ($b/h = 0.75$). For each masonry wall, the unreinforced configuration (URS) was compared with two resisting schemes: concrete ring beams (RSB) and steel chains (RSC). Therefore, a total of 9 types of masonry walls were considered which differ in terms of geometry and resistance mechanisms. To perform the pushover analyses, the finite element technique was employed by using three different load distributions. The results expressed in terms of inner forces on the piers and spandrels were subsequently compared with the formulae for flexural and shear strength provided by IBC. The comparisons showed that the reliability of these equations is at least questionable, especially for the prediction of the spandrels' strength. In this case, the strength models provided by the Standards underestimate by a large amount the real strength both for the unreinforced and the strengthened walls, especially in the case of slender spandrels in strengthened walls.

1. Introduction

A large amount of masonry buildings in Italy and Europe are located in earthquake prone areas and most of them were built before the development of modern rules for seismic design. In many cases, being historic buildings, they have a significant social value and the evaluation of their seismic capacity and safety is still an open scientific issue.

Typically, these constructions are composed of load bearing masonry walls disposed along two orthogonal directions and connected by means of flexible floor diaphragms. Observation of the damages suffered during past seismic events has highlighted that in most cases failure of these buildings is due to out-of-plane behaviors of the walls [1]. In cases where out-of-plane collapse mechanisms have been prevented by proper structural strengthening, as steel chains or reinforced concrete (RC) ring beams, collapses due to in-plane failure were observed [2]. In the latter mechanism, the strength of the walls depends on many geometric and mechanic

* Corresponding author.
E-mail addresses: michele.betti@unifi.it (M. Betti), luciano.galano@unifi.it (L. Galano), frapalru@fis.upv.es (F.J. Pallarés).

https://doi.org/10.1016/j.engfailanal.2023.107430
Received 4 April 2023; Received in revised form 10 June 2023; Accepted 24 June 2023
Available online 25 June 2023

factors such as: the disposition of the openings in the walls, the characteristics of mortar and units, the masonry texture, the stress level due to the dead loads, the presence of local reinforcements, the boundary conditions, the coupling between masonry piers and spandrels, etc. ([3,4,5,6,7,8,9]). Shear walls with regularly spaced openings are composed of piers (masonry columns) and spandrels (masonry beams) so their behavior under in-plane seismic actions is similar to the behavior of the RC framed structures, and the strength of each wall strongly depends on that of such elements.

The scientific literature offers consistent numerical approaches to estimate the seismic strength of masonry walls. Some of them refer to the finite element (FE) method, using proper constitutive laws to simulate the masonry behavior ([10,11,12,13]). These techniques are very efficient but computationally expensive and require expert users and advanced software, which make them difficult to use for practitioners. Alternative approaches have been also proposed based on the so-called macro-element models. The walls are partitioned in a certain number of components (one or two-dimensional macro-elements) depending on the structural compound geometry and shape ([14,15,16,17]). Some of these methods adopt the scheme of no-tension material (NTM) for masonry, and the solution is obtained by an iterative procedure. Methods as POR, originally proposed by Tomazevic in 1978 ([18,19]), and the more recent equivalent frame methods as implemented in the SAM code belong to this category ([20,21,22]).

Even if they are simpler than the FE technique, these approaches require dedicated software to solve the iterative steps needed by the solution procedures. Besides, reliable strength and deformability models for masonry piers and spandrels have to be used anyway. These masonry elements bear the static loads and, during earthquakes, are subjected to additional shear, bending and axial forces. Experimental tests and refined numerical simulations have been extensively performed, especially for piers, showing three main failure mechanisms ([23,24,25]): a) flexural failure, i.e. cracking of the masonry in tension, and consequent crushing of the diagonally opposite compressed corner of the element; b) shear failure by diagonal cracking; and c) shear sliding failure. One major result of these studies is the proposal of simplified models and formulae to estimate strength and deformability of the panels ([26,27,28]).

A critical issue is the reproduction of the actual boundary conditions of the masonry panels (piers and spandrels) inside the walls ([4,29,30,31,32,33,34,35]). These boundary conditions are uncertain, as they modify during the loading process, and thus very difficult to evaluate and reproduce numerically.

The analyses presented in this paper, although not refined in simulating the behavior of each panel, have the advantage to accurately represent the current distribution of the inner forces in the walls appropriately simulating the boundary conditions of the masonry panels. Overall, 9 typologies of walls with regular geometry were modeled by the FE method. The walls represent the typical façades of existing masonry buildings in old towns, hence a brick masonry with poor mechanical properties was considered. The walls differ in the span-to-height ratio b/h of the masonry beams: a) slender beams ($b/h = 2.0$); b) intermediate beams ($b/h = 1.00$) and c) short beams ($b/h = 0.75$). In addition, for each masonry wall, the unreinforced configuration (denoted as URS) whereby only concrete lintels over the windows were assumed, was compared with two common strengthening schemes: concrete ring beams (RSB) or steel chains (RSC). Three different horizontal load distributions were also considered: i) loads proportional to the masses (g analyses), ii) loads proportional to the masses multiplied by the heights (h analyses) and iii) loads proportional to the masses multiplied by the displacements of the first in-plane mode shape (s analyses). Therefore, a total of 27 pushover analyses were performed to reproduce the behavior of the 9 masonry walls up to their maximum base shear. Inner forces on the masonry piers and spandrels for the unreinforced and strengthened walls were compared with the formulae for flexural and shear strength provided by IBC ([36,37]) to have an insight on their reliability. This comparison shows that the reliability of these equations is at least questionable, especially for the prediction of the strength of the spandrels. In this case, the strength models provided by the Standards underestimate by a large amount the real strength both in the unreinforced and the strengthened walls. This was especially true in the case of slender spandrels in strengthened walls. Since the strength models adopted by IBC are substantially similar to the ones proposed by the ES, conclusions can be drawn for both Standards.

The paper is organized as follows: Section 2 reports and discusses the strength models proposed in literature for the masonry piers and spandrels. Section 3 shows the geometries of the analyzed masonry walls, reports the assumed mechanical properties, and describes the FE models together with the damage and failure criteria adopted for the masonry. Finally, Section 4 discusses the main results obtained from the numerical analyses and compares them with the formulae available in literature, thus providing insights on their reliability. The main conclusions of this study are summarized in Section 5.

2. Strength models for masonry piers and spandrels

Consider a plane masonry wall with openings regularly spaced subjected to the self-weight and the static loads of floors and roof. In the seismic analysis based on the macro-elements models, the wall is modeled as an equivalent frame composed of piers, spandrels, and nodes (Fig. 1).

In the standard pushover methods, the seismic loading process is represented by a set of horizontal monotonically increasing loads applied at each floor. Fig. 2 shows a generic masonry pier extracted by the wall in static and seismic configurations (h = height, b = width, s = thickness of the pier; in this scheme the self-weight is not taken into account for sake of simplicity). Shear force V, axial force N, and bending moment M act in the bottom and top sections as in a beam.

As the seismic load increases, such panel initially cracks in complex ways subsequently reaching the ultimate strength, i.e. the maximum shear V_u, followed by large deformations and decreasing of shear (softening behavior). The representation of the shear force V vs. the displacement δ diagram is crucial for the use of a macro-elements model.

A spandrel can be simply considered as a pier rotated by 90°, although with significant differences due to the low level of the axial force and the different orientation of the axis with respect to the masonry texture.

The piers and spandrels strength models proposed by IBC ([36,37]) for masonry walls with regular texture here considered are

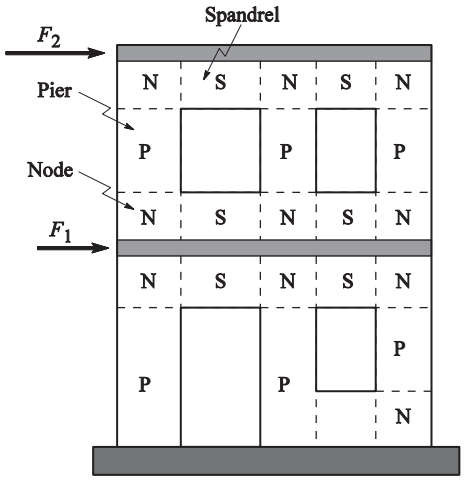

Fig. 1. Idealization of a masonry wall by an equivalent frame (P = pier; S = spandrel; N = node).

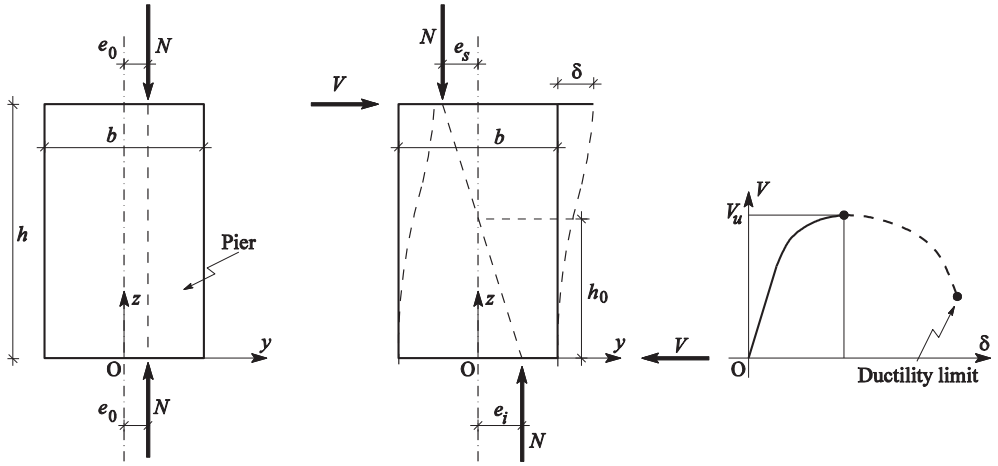

Fig. 2. Inner forces in a masonry pier in static and seismic configuration.

reviewed and commented next (the partial safety factors using the average strengths of the materials have not been considered, as requested for nonlinear analyses).

2.1. Masonry piers

The flexural strength of a pier in a generic section is given by:

$$M_u = \frac{b^2 s \sigma_0}{2}\left(1 - \frac{\sigma_0}{\chi f_w}\right), \tag{1}$$

where f_w denotes the compressive strength of the masonry, $\sigma_0 = N/(bs)$ is the average vertical stress (positive in compression) and χ is a shape factor equal to 0.85 ([36]). Eq. (1) disregards the tensile strength of the masonry and is valid if $\sigma_0 \geq 0$, while M_u is set equal to zero if $\sigma_0 < 0$, so it slightly underestimates the flexural strength for low levels of compression. Then, a second formula is considered:

$$M_u = \frac{b^2 s}{6}(f_t + \sigma_0), \tag{2}$$

where f_t is the tensile strength of the masonry, mainly depending on the mortar quality. Eq. (2) is valid if $\sigma_0 \geq -f_t$, and simply characterizes the cracking limit state in the considered section. In this paper, Eq. (1) was assumed for the flexural strength, considering the value provided by Eq. (2) in the zones of low or negative σ_0. The ultimate shear V_{uf} associated to M_u depends on the height h_0 (see Fig. 2) of the inflection point of the pier axis (h_0 is highly variable with the boundary conditions and is not univocally definable).

IBC considers two alternative methods to evaluate the shear strength of a pier in old buildings made of masonry with regular texture.

In the first case, the failure for diagonal cracking based on the classical formula proposed by Turnsek and Cacovic in 1970 [38] is considered:

$$V_{us1} = rbs\frac{f_t}{\beta}\sqrt{1+\frac{\sigma_0}{f_t}}, \tag{3}$$

in which β is a shape factor which takes into account the actual distribution of the shear stresses in the mid-height section of the pier. The parameter r, an over-strength factor introduced in this paper, is not present in the original formulation. In Eq. (3), the strength f_t actually reflects an equivalent tensile strength of the masonry related to the cracking in direction of the principal tensile stress at the center of the panel (it has been assumed as in Eq. (2)).

The original formulation sets $\beta = 1.5$ - according to the Saint Venant's theory - and $r = 1$, so in this case Eq. (3) effectively corresponds to the initial cracking state at the center of the pier. Although IBC sets $\beta = h/b$ in the range 1.0–1.5, and does not take into account the factor r, to evaluate V_{us1} a fixed value 1.5 for β [25] and a factor r greater than one as in [39] were assumed. A similar criterion can be used to limit the principal compressive stress at the center of the pier, i.e. V_{us1} is limited by:

$$V_{us1} \leqslant bs\frac{f_w}{\beta}\sqrt{1-\frac{\sigma_0}{f_w}}, \tag{4}$$

which is relevant for high compression σ_0. In old buildings this situation is infrequent, and actually the Eq. (4) instance has never occurred in the numerical analyses reported next.

In masonry with regular texture, it could be more appropriate to consider a diagonal crack that propagates along the mortar joints, i.e. the bed and the vertical joints. To this purpose, the following formula is suggested in [37]:

$$V_{us2} = \frac{bs}{\beta}\left(\frac{f_{v0}}{1+\mu_s\phi_s}+\frac{\mu_s\sigma_0}{1+\mu_s\phi_s}\right), \tag{5}$$

in which f_{v0} is the mean cohesive strength of the mortar joints, μ_s is the friction coefficient and $\phi_s = h_b/l_s$ is the average slope of the crack (h_b = height of the blocks, l_s = length of overlap of blocks in two consecutive layers). Strength V_{u2} has to be also limited to consider the fracture of the blocks, by:

$$V_{us2} \leqslant \frac{bsf_{bt}}{2.3\beta}\sqrt{1+\frac{\sigma_0}{bf_{bt}}}, \tag{6}$$

where f_{bt} is the average tensile strength of the blocks. Hence, according to this model, V_{us2} was assumed as the minimum between Eqs. (5) and (6). Finally, for new masonry walls, [36] adopts a different model to predict the shear strength of a pier, i.e. failure by sliding in the bottom or in the top section:

$$V_{us3} = b's(f_{v0}+\mu\sigma_n), \tag{7}$$

where $b' = b$ and $\sigma_n = \sigma_0$ if $e = |M/N| \leq 1/6$, while $b' < b$ and $\sigma_n = N/(b's)$ if $1/6 < e < 1/2$. V_{us3} is based on the standard Coulomb formula, in which the shear stresses develop only in the compressive zone of the section with the friction μ (generally different from μ_s). The length b' can be simply evaluated considering a linear distribution of the normal stresses over the sliding section. In any case V_{us3} is limited by:

$$V_{us3} \leqslant \frac{0.065f_b}{0.7}, \tag{8}$$

where f_b is the compressive strength of the blocks. Since this paper is focused on old masonry walls, Eqs. (7) and (8) were not considered, and the shear strength was assumed in the two alternative ways equal to V_{us1} and V_{us2}.

2.2. Masonry spandrels

With respect to the strength models of spandrels, IBC distinguishes between elements in which the axial force N is known or unknown. If N is known the same strength models of piers can be applied, although the shear strength by sliding failure (Eq. (7)) is not considered for old buildings. If N is unknown, a minimum strength needs to be assessed that implies two further cases. If the spandrel is unreinforced, or there is only a lintel (the URS case), evaluation of the strength is obtained by the cohesion of the mortar joints and by a safety evaluation of the normal stresses in the vertical end sections. On the contrary, if the spandrel is reinforced by a ring beam or a steel chain passing through (the RSB and RSC cases), since a strut-and-tie mechanism can develop through the panel, the strength is increased. In this study, N was assumed to be known, as it was obtained by the pushover analyses. As will be reported next, N is always very low (or even a traction), consequently minimum strength values were fixed.

In this paper, the flexural strength was assumed as given by Eqs. (1) and (2), replacing b with h, f_w with f_h (the masonry compressive strength in the horizontal direction) and f_t with f_{tf}:

$$f_{tf} = \min\left(\frac{f_{bt}}{2},\ f_{v0}+\frac{\mu_s\sigma_y}{\phi_s}\right). \tag{9}$$

In Eq. (9) f_{bt} is the tensile strength of the blocks, σ_y is the average compressive stress in the considered vertical end section, μ_s is the

friction coefficient and ϕ_s the interlock coefficient ([37]). Minimal flexural strengths were used for unreinforced and reinforced spandrels, given by respectively:

$$M_u \geqslant M_{u\min} = \frac{h^2 s}{6} f_{tf},$$

$$M_u \geqslant M_{u\min} = \frac{H_p h}{2}\left(1 - \frac{H_p}{\chi h s f_h}\right),$$

$$H_p = \min(0.4 h s f_h,\ T_s). \tag{10}$$

In Eq. (10), T_s is the maximum allowed tensile force of the horizontal tie elements (which will be discussed in the next Section). To summarize, the flexural strength of spandrels was given by Eqs. (1) and (2) as for the piers, with the limits given by Eq. (10). A shear strength $V_{uf\min}$ was associated to $M_{u\min}$, as

$$V_{uf\min} = \frac{2M_{u\min}}{b}, \tag{11}$$

which is related to an axisymmetric structural scheme.

Similarly, the two shear strengths V_{us1} and V_{us2} were evaluated by Eq. (3), (5) and (6) replacing b with h. Two minimum shear strengths were also considered, obtained by the same formulae setting $\sigma_0 = 0$ without differences between unreinforced and reinforced spandrels:

$$V_{us1} \geqslant V_{us1\min} = rhs\frac{f_t}{\beta},$$

$$V_{us2} \geqslant V_{us2\min} = \min\left(\frac{hs}{\beta}\left(\frac{f_{v0}}{1+\mu_s\phi_s}\right),\ \frac{bsf_{bt}}{2.3\beta}\right). \tag{12}$$

The minimum shear strength of a spandrel was finally assumed as $V_{us\min} = \min(V_{uf\min}, V_{us1\min}, V_{us2\min})$, reducing also $M_{u\min}$ of Eq. (10) according to Eq. (11) if $\min(V_{us1\min}, V_{us2\min}) \leq V_{uf\min}$.

To summarize, the strength models used for spandrels were the same as those used for piers considering additional specific minimum strengths.

3. Masonry walls and FE discretization

3.1. Geometry of the walls

Fig. 3 shows the three different geometries of the masonry walls analyzed. They are 17.00 m long, 15.00 m high, have a thickness of 0.45 m and are typical of the external façades in old masonry buildings with regular openings. They have ground floor and four elevated stories: all the piers have a width of 1.40 m, and all the spandrels have a clear span of 1.20 m. In type A wall, the spandrels of the floors are 0.6 m high (slenderness $b/h = 2.0$), while in type B and C walls the slenderness is 1.0 and 0.75, respectively. In the schematization of each wall as an equivalent frame, there are 35 piers and 24 spandrels numbered as reported in Fig. 3.

Walls were made of full bricks masonry and poor lime mortar, as is usually observed in old buildings in historic centers (Table 1). Three different cases of reinforcement were considered for each of them. In the first case, there is only a concrete lintel 200 mm high over each opening (walls with unreinforced spandrels, URS); in the second case, there is also a RC ring beam 200 m high and 450 mm thick at each floor (four steel bars with a diameter of 10 mm reinforced the corbels, walls RSB). Lastly, in the third case, the spandrels are reinforced by steel chains of a diameter of 26 mm (walls RSC, Table 2). Compressive strength f_c of 38 N/mm^2 for concrete, yield strength σ_s of 300 N/mm^2 for steel chains and an actual stress in the chains of $2\sigma_s/3$ were considered thus resulting in a tensile force T_s = 106.200 kN (see Table 2; the same T_s was assumed for each RC corbels).

A load of $q = 4$ kN/m^2 acting for a depth of 2.5 m was applied to each level and to the roof to simulate the dead weight of the floors and the live loads. As an example, Fig. 4 shows the two walls of type B, reinforced by the corbels and by the steel chains.

3.2. Mechanical properties of the masonry

A full brick and poor lime mortar masonry texture, typical of the buildings in historic city centers was considered ([40,41]). Table 1 resumes the selected parameters that deserve a few comments. Many values are in agreement with the suggestions of [37], others were taken as representative of this masonry typology. Considering $f_b = 10$ N/mm^2, mortar strength $f_m = 0.5$ N/mm^2, $f_{bt} = f_b/20$, a ratio of 0.4 between the joint thickness ($t_m = 20$ mm) and the height of the bricks ($h_b = 50$ mm), and a uniformity coefficient equal to 2, the Hilsford's formula gives $f_w = 1.86$ N/mm^2. The compressive strength $f_w = 1.52$ N/mm^2 is slightly different, but it was selected to be consistent with the FE model. For brick masonry and lime mortar, [37] suggests a range of 2.6–4.3 N/mm^2 for f_w. A reduction coefficient of 0.7 × 0.7 must be however used for thickness of mortar joints greater than 13 mm and strength mortar lower that 0.7 N/mm^2, as in the present case. f_t and f_{v0} agree with [37], but also f_t is consistent with the FE model. A coefficient of 0.7 was applied to f_w to obtain f_h. Factor r in Eq. (3) was set equal to 1.1 according to the results obtained in [39]. The coefficient μ_s was fixed as suggested in

[37] and, for a standard brick length overlap of 125 mm, $\phi_s = 0.4$.

Table 2 resumes the geometrical and mechanical parameters of the concrete of the lintels, of the corbels and of the steel of the chains. A_s denotes the area of each steel chain (diameter $\phi = 26$ mm) and σ_s is the steel yield stress (other symbols are explained next).

As an example, Fig. 5 represents the flexural and the shear strengths vs the axial force for a masonry pier in dimensionless form, according to the models reported in the previous section and to the values in Table 1. Similarly, Fig. 6 represents the same domains for a spandrel with dimensions $b = h = 1200$ mm.

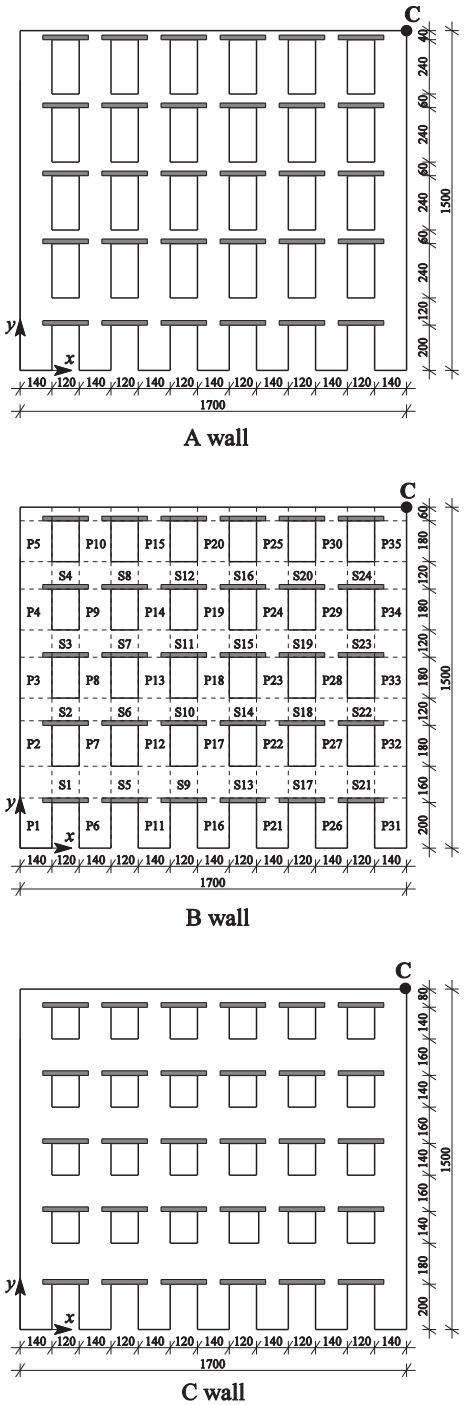

Fig. 3. Geometry of the considered masonry walls (URS case).

Table 1
Geometrical and mechanical properties of brick and lime mortar of masonry (E_w = longitudinal modulus of elasticity, G_w = tangential modulus of elasticity, γ_w = specific weight).

f_w (N/mm^2)	1.52
f_t (N/mm^2)	0.15
f_{tf} (N/mm^2)	0.25
f_{v0} (N/mm^2)	0.20
f_h (N/mm^2)	1.06
f_b (N/mm^2)	10.0
f_{bt} (N/mm^2)	0.5
f_m (N/mm^2)	0.5
t_m/t_b	0.4
β	1.5
r	1.1
μ	0.4
μ_s	0.577
ϕ_s	0.4
E_w (N/mm^2)	2000
G_w (N/mm^2)	800
γ_w (kN/m^3)	18.0

Table 2
Geometrical and mechanical properties of concrete and steel (E_c = longitudinal modulus of elasticity of concrete, G_c = tangential modulus of elasticity of concrete, γ_c = specific weight of concrete).

f_c (N/mm^2)	38.0
f_{ct} (N/mm^2)	2.9
E_c (N/mm^2)	33,000
G_c (N/mm^2)	13,750
γ_c (kN/m^3)	25.0
σ_s (N/mm^2)	300
A_s (mm^2)	531
E_s (N/mm^2)	206,000
G_s (N/mm^2)	78,267
γ_s (kN/m^3)	78.5
$T_s = 2\sigma_s A_s/3$ (N)	106,200

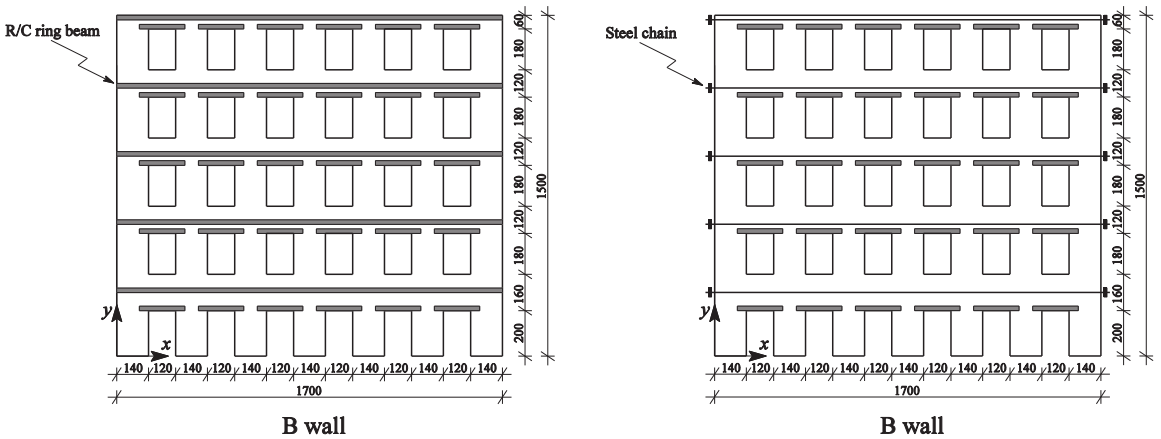

Fig. 4. Geometry of the type B masonry walls reinforced by corbels (RSB, left) and steel chains (RSC, right).

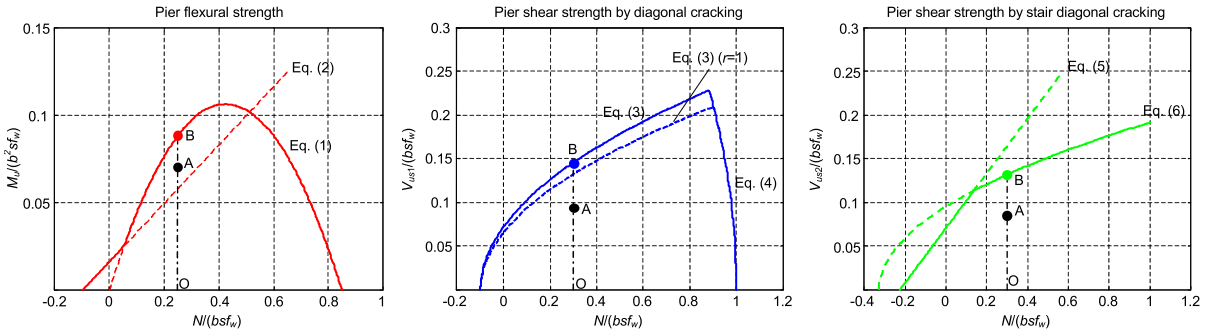

Fig. 5. Flexural and shear strength domains for a masonry pier in dimensionless form (see Table 1 for relevant parameters).

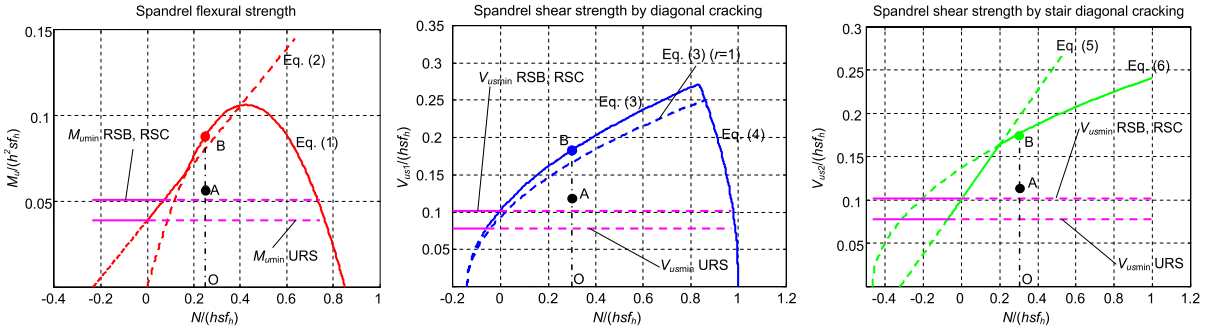

Fig. 6. Flexural and shear strength domains for a masonry spandrel in dimensionless form (see Table 1 and Table 2 for relevant parameters).

In these figures, if point O represents the level of the normal stress acting in the masonry panel (pier or spandrel), point A denotes the value of the actual action (moment or shear) corresponding to the level of normal stress O, while B represents the ultimate strength value predicted by the formulae summarized in Section 2.

3.3. Numerical model of the walls

The walls were discretized by FE using the commercial code ANSYS [42]. The eight node isoparametric element called *Solid65* was used to discretize the masonry walls, the lintels and the RC corbels, with a mesh size of about 200 mm. Standard linear elastic tie elements were used to reproduce the steel chains.

Masonry was modelled as a homogeneous and isotropic material by using a smeared crack approach. In particular, the plasticity model based on the Drucker-Prager yield surface [43] was used to simulate the plastic deformations of the masonry in compression, while the Willam-Warnke [44] failure criterion was adopted to rule the cracking phenomenon.

This constitutive model requires to identify the following parameters: the elastic moduli E and G, the cohesion c, the friction angle φ, the dilatancy angle δ for the Drucker-Prager model, and the compressive and the tensile strengths f_{cWW} and f_{tWW} for the Willam-

Table 3
Elastic, Drucker-Prager and Willam-Warnke criteria parameters, with symbols related to the FE models.

		Masonry	RC
Elastic parameters	E (N/mm^2)	2000	33,000
	G (N/mm^2)	800	13,750
	γ (kN/m^3)	18.0	25.0
Drucker-Prager criterion	c (N/mm^2)	0.24	2.80
	δ (°)	55	37
	φ (°)	55	32
	f_{cDP} (N/mm^2)	1.52	11.23
	f_{tDP} (N/mm^2)	0.22	3.73
Willam-Warnke criterion	f_{cWW} (N/mm^2)	4.00	38.00
	f_{tWW} (N/mm^2)	0.15	2.9
	β_c (first coeff. for shear stresses on crack planes)	0.75	0.75
	β_t (second coeff. for shear stresses on crack planes)	0.25	0.25

Warnke criterion. In the Drucker-Prager model, for every choice of c and φ, correspond the compressive and tensile uniaxial strengths, here denoted as f_{cDP} and f_{tDP} (the intersections of the yield surface with the coordinate axes). An appropriate choice of these parameters allows to obtain an equivalent material in which f_{tWW} is lower than f_{tDP} while f_{cWW} is greater than f_{cDP} so a cut-off to the tensile stresses is introduced, maintaining the plastic behavior in compression [45]. Hence, in this model, f_{cDP} and f_{tWW} represent the compressive and tensile uniaxial strengths of the masonry. The same model was used for RC lintels and corbels.

Table 3 resumes the selected parameters for the two materials.

4. Discussion of the results

FE models were used to perform the pushover analyses.

In the first phase the static loads and a tensile force to each steel chain were applied. As is known, this tie force is variable over time and difficult to be predicted, so in these analyses an initial representative value was used, corresponding to a fraction of 1/3 of the yield steel strength (corresponding to a stress of $\sigma_s/3 = 100$ N/mm^2). The tie force T_s used in the strength models of spandrels was instead assumed as reported in Table 2, corresponding to a steel stress of $2\sigma_s/3 = 200$ N/mm^2 to reflect the increase observed in the pushover analyses.

Table 4
Results of the pushover analyses.

Case	Wall	V_{bmax} (kN)	u_{xC} (mm)	V_{bmax}/W	piers				spandrels			
					$\lvert\gamma_1\rvert_{max} \times 10^3$		$\lvert\gamma_2\rvert_{max} \times 10^3$		$\lvert\gamma_1\rvert_{max} \times 10^3$		$\lvert\gamma_2\rvert_{max} \times 10^3$	
1	A-URS-g	427.81	19.2	0.188	0.45	31	0.75	31	0.74	17	**1.61**	10
2	A-URS-h	314.65	21.0	0.138	0.41	28	0.80	28	0.96	21	**2.03**	18
3	A-URS-s	322.13	31.3	0.142	0.56	19	**1.11**	19	**2.44**	18	**5.69**	18
4	B-URS-g	521.60	10.3	0.216	0.40	20	0.62	20	0.87	21	**1.04**	21
5	B-URS-h	334.53	6.9	0.138	0.18	25	0.30	31	0.41	21	0.50	15
6	B-URS-s	385.39	12.5	0.160	0.32	24	0.49	24	**1.22**	21	**1.44**	21
7	C-URS-g	581.36	6.1	0.232	0.40	31	0.67	31	0.49	21	0.57	21
8	C-URS-h	401.35	10.0	0.160	0.49	20	0.65	20	0.93	18	**1.11**	18
9	C-URS-s	419.49	12.4	0.167	**1.02**	25	**1.36**	25	**1.00**	18	**1.19**	18
10	A-RSB-g	620.47	11.7	0.266	0.58	27	**1.15**	27	0.89	21	**1.18**	21
11	A-RSB-h	468.88	14.5	0.201	0.65	27	**1.29**	27	0.82	21	**1.33**	6
12	A-RSB-s	445.76	13.9	0.191	0.72	27	**1.43**	27	**1.19**	18	**2.79**	18
13	B-RSB-g	770.67	6.9	0.312	0.49	16	0.83	16	0.32	21	0.39	21
14	B-RSB-h	662.36	8.9	0.268	0.46	12	0.72	12	0.33	17	0.42	14
15	B-RSB-s	626.50	6.9	0.254	0.32	21	0.54	21	0.28	18	0.38	18
16	C-RSB-g	796.60	6.0	0.311	0.59	26	0.99	26	0.26	21	0.30	21
17	C-RSB-h	730.11	7.2	0.285	0.43	21	0.72	21	0.29	14	0.34	14
18	C-RSB-s	719.34	6.7	0.281	0.45	31	0.75	31	0.28	17	0.32	14
19	A-RSC-g	620.96	13.6	0.271	0.39	27	0.77	27	0.87	21	**1.91**	10
20	A-RSC-h	466.67	13.6	0.203	0.30	18	0.60	18	0.83	14	**1.93**	14
21	A-RSC-s	461.73	13.2	0.201	0.31	27	0.61	27	0.90	18	**2.09**	18
22	B-RSC-g	735.22	6.5	0.302	0.41	21	0.69	21	0.45	21	0.54	21
23	B-RSC-h	673.05	12.8	0.277	0.74	13	**1.14**	13	0.87	14	**1.16**	14
24	B-RSC-s	656.67	9.5	0.270	0.51	13	0.79	13	0.73	21	0.96	18
25	C-RSC-g	796.92	6.2	0.315	0.59	16	**1.00**	16	0.37	17	0.43	17
26	C-RSC-h	672.99	7.9	0.266	0.61	26	**1.02**	26	0.53	10	0.63	10
27	C-RSC-s	691.49	7.2	0.274	0.48	26	0.81	26	0.50	10	0.60	10

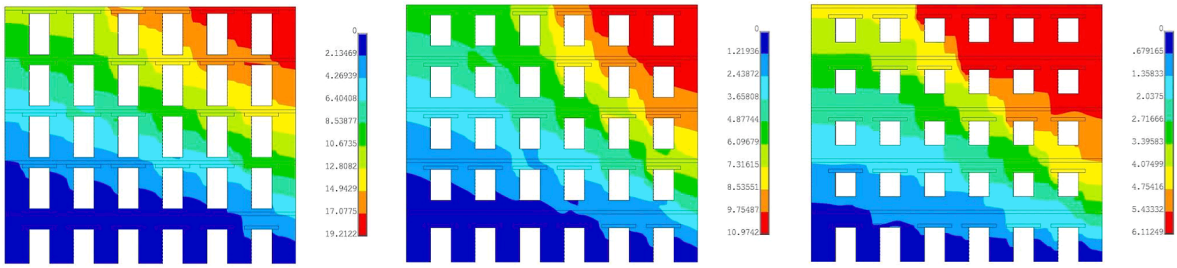

Fig. 7. Displacements of the walls A-URS-g, B-URS-g and C-URS-g at the last step of the analyses (measures in mm).

In the second phase, a set of distributed horizontal loads was applied at each node of the mesh in three different ways: i) loads proportional to the masses (g analyses), ii) loads proportional to the masses multiplied by the heights (h analyses), and iii) loads proportional to the masses multiplied by the displacements of the first mode shape (s analyses). Given the purpose of this paper, the nonlinear analyses were performed under load control and the magnitude of the horizontal loads was monotonically increased to simulate the ascending branch of the capacity diagrams. Table 4 collects the results of all the 27 pushover analyses (as an example A-URS-g is the wall with slender spandrels, not reinforced with horizontal loads of type g) and Fig. 7 shows the final pattern of displacements for the A-URS-g, B-URS-g and C-URS-g walls.

4.1. Global behavior of the walls

The seismic behavior of the walls was first analyzed in terms of resultant of the horizontal load at the base and displacement at the roof level. Some diagrams of base shear V_b normalized to the total weight W vs the horizontal displacement u_{xC} of the control point C (the right upper corner of the walls, Fig. 3) are presented in Fig. 8 that shows the capacity diagrams of the cases g and h (cases s are similar to the corresponding cases h, and are not presented in the figure). The complete set of results is collected in Table 4, while Table 5 reports the mechanism corresponding to the last step of the pushover analyses by summarizing the most damaged panels (divided between piers and spandrels at each floor). For URS walls the ratio of maximum base shear to wall weight was in the range of

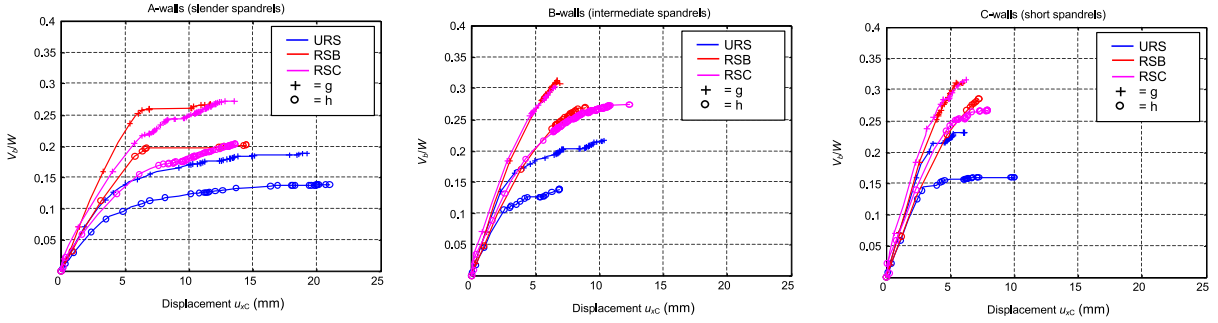

Fig. 8. Diagrams of base shear vs the horizontal displacement of the control point C (see Fig. 3).

Table 5
Localization of damage.

Case	Wall	Piers(*)	Spandrels(*)
1	A-URS-g	-	1-2-3
2	A-URS-h	-	1-2-3
3	A-URS-s	-	1-2-3-4
4	B-URS-g	GF-1	1-2
5	B-URS-h	GF-1	1
6	B-URS-s	GF	1-2-3
7	C-URS-g	GF-1-2	1-2
8	C-URS-h	GF-1-2-3	2
9	C-URS-s	1-2-3	1-2-3
10	A-RSB-g	GF-1	1-2
11	A-RSB-h	1	1-2-3
12	A-RSB-s	1	1-2-3
13	B-RSB-g	GF	1
14	B-RSB-h	GF-1-2	1-2
15	B-RSB-s	GF-1-2	1-2
16	C-RSB-g	GF	-
17	C-RSB-h	GF-1	1-2
18	C-RSB-s	GF	1
19	A-RSC-g	GF-1	1
20	A-RSC-h	GF-1-2	1
21	A-RSC-s	GF-1-2	1
22	B-RSC-g	GF	1
23	B-RSC-h	GF-1-2	1-2
24	B-RSC-s	GF-1-2	1-2
25	C-RSC-g	GF	1
26	C-RSC-h	GF-1-2	1-2
27	C-RSC-s	GF-1-2	1-2

(*) Floors with prevalent damage in terms of cracking patterns, GF = ground floor.

Fig. 9. Cracking patterns of some walls in the last step of the pushover analysis.

0.14–0.23 with higher values in the type C wall with short spandrels. This ratio increased up to 0.19–0.31 for the RSB walls (reinforced with the corbels) and up to 0.20–0.31 for the RSC walls (reinforced with the steel chains). Effectiveness of the corbels and steel chains in terms of increased strength is evident in all cases; the increase of stiffness was significant only for walls with slender spandrels.

The maximum normalized displacements u_{xC}/H were in the range from 0.33‰ (for the strengthened walls with short spandrels) to 2‰ (for the unreinforced walls with slender spandrels). These displacements were relatively small, nevertheless the analyses were appropriately extended to obtain diffuse cracking patterns. Some examples of these patterns are reported in Fig. 9.

In the A-URS-h wall, the spandrels were greatly damaged, and the piers behaved as ideal corbels. The collapse affected especially the spandrels of the first three floors and the piers of the low right corner (flexural collapse). Overall, the damage was extended to many elements. In the C-URS-h wall with short spandrels, the damaged elements followed an ideal inclined strut that developed from the low right corner, while the elements external to it were nearly undamaged. Some spandrels collapsed by shear for diagonal cracking. For the A-RSB-h and C-RSB-h walls reinforced by the corbels, a floor collapse mainly concentrated on the first level was rather evident. The piers and the spandrels at the first level in the case of C-RSB-h collapsed by diagonal cracking. Overall, given the higher structural stiffness, the corbels produce a damage uniformly distributed along the width of all the floors. The cracking patterns in the A-RSC-h and

C-RSC-h walls, reinforced by steel chains, were similar to the corresponding walls reinforced by the corbels. The cracking patterns show that only in a small number of elements the collapse mode was clearly evident; in most cases the cracks were irregularly located and a specific failure mode was not detectible.

Results of the FE analyses allowed the calculation of the shear strain for piers and spandrels. Generally, beam equivalent models are used to this aim. Consider a linear elastic beam with constant transversal section (A = area J = moment of inertia, χ_y = shear factor) and clear span h, and denote with v_i, v_j, θ_i and θ_j the deflections and the rotations of the end sections. If E and G are the elastic moduli, in the hypothesis of constant shear along the axis, the absolute shear strain γ_1 is given by:

$$|\gamma_1| = \left| \left(\frac{v_j - v_i + \left(\theta_i + \theta_j\right)\frac{h}{2}}{\left(\frac{h\chi_y}{GA} + \frac{h^3}{12EJ}\right)} \right) \right| \frac{\chi_y}{GA}. \tag{13}$$

The same model used for a beam without flexural deformation gives two values:

$$|\gamma_{1i}| = \left|\frac{v_j - v_i}{h} + \theta_i\right|,$$

$$|\gamma_{1j}| = \left|\frac{v_j - v_i}{h} + \theta_j\right|. \tag{14}$$

Since in this case the rotation θ has to be constant, Eq. (14) are theoretically correct only if $\theta_i = \theta_j$. To adjust this model to a beam in which the end rotations are different, the following index

$$|\gamma_2| = \left|\frac{v_j - v_i}{h} + \frac{\theta_i + \theta_j}{2}\right|, \tag{15}$$

is a reasonable approximation. Eq. (15) is the same of Eq. (13) if $EJ \to \infty$. [37] defines two shear deformations, called chord rotations, one for each end section of a panel, depending on the position of the inflection point of the axis and the shear span; in the hypothesis that the shear span is equal to $h/2$ as approximately occurs in the spandrels (h is b, in this case) the mean of the two values is equal to γ_2. The index γ_2 is more reliable than γ_1 because it is independent from the elastic moduli, and it is better related with the deformation of a panel rather than γ_1.

Table 4 collects the absolute maximum values of γ_1 and γ_2 for each analysis (for both piers and spandrels) together with the elements in which such values occurred. These quantities were evaluated by the horizontal and the vertical displacements of the four corners of each panel obtained by FE results. Table 4 highlights in bold the strains greater and/or equal to 1×10^{-3}. They are useful to calibrate the macro-elements model. As an example, the pier 27 of the A-RSB-h wall has $|\gamma_2|_{max}$ equal to 1.29×10^{-3}. Supposing that this state corresponds to the point of maximum shear, and setting the local ductility factor to 5, the ultimate shear strain γ_{2u} has to be equal to 6.45×10^{-3}. Otherwise, if the values of the ultimate shear strain suggested by [37] (1.0×10^{-2} and 0.5×10^{-2} for flexural and shear collapse in the pushover analyses for the so called limit state of collapse, LSC) are assumed, it is possible to obtain the minimal required ductility factor equal to 7.75 and 3.88, respectively. Although such allowed ductility have been extensively investigated by experimental tests, the FE simulations take more properly into account the effective boundary conditions of piers and spandrels assembled in the wall.

4.2. Analysis of inner forces in piers and spandrels

Results of pushover analyses provided the axial force N, the shear force V and the bending moment M at the end sections of each pier and spandrel. In particular, for spandrels, the stresses in the lintels and the corbels were considered together with the stresses of the masonry elements in each section. Hence, N, V and M also included the contribution of the concrete elements.

The evolution of the wall cracking patterns showed that only in few cases the panels displayed a specific collapse mode. In some of these instances a diagonal cracking pattern was observed, sometimes followed by a flexural collapse, especially in piers. However, in most cases the evolution of cracks does not follow a precise geometric scheme and no one specific collapse mode was observed. Nevertheless, the value of the inner forces has to be compared with proper quantities and to this aim the strength models summarized in Section 2 have been considered.

With reference to Fig. 5 and Fig. 6 and to the flexural strength domains $M - N$, for a generic analysis and panel, the maximum ratio between the actual bending moment (OA) and the strength moment (OB) corresponding to the same axial force defined as

$$\rho_{fx} = \frac{\mathrm{OA}}{\mathrm{OB}}, \tag{16}$$

was assumed as a parameter representing the bending effort of the panel (considering the maximum value between the top and the bottom section). Similarly, Eq. (16) was used to obtain ρ_{s1} and ρ_{s2} for the two shear strength domains $V - N$, considering the mid-height section for piers and the mid-span section for spandrels. As an example, Fig. 10 shows the maximum bending moments and shear forces for the 35 piers in the B-RSB-g wall, represented with the corresponding strength models. The maximum ratios calculated by Eq. (16) were $\rho_{fx} = 1.87$, $\rho_{s1} = 0.83$ and $\rho_{s2} = 0.96$. In this case the piers of the first floor with the higher axial forces developed the full flexural strength or in any case the bending moments were beyond the limit defined by Eq. (1), thus denoting a flexural collapse of these

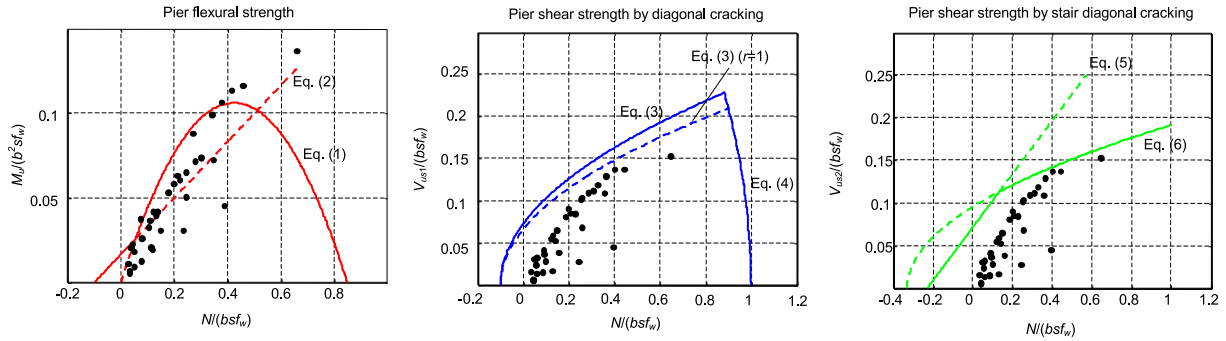

Fig. 10. Flexural and shear strength domains together with bending moments and shear forces for the masonry piers of the wall B-RSB-g in dimensionless form.

elements. In the same piers, the shears were slightly lower than the strengths predicted by Eqs. (3) and (5), thus suggesting that a typical full shear collapse was not reached. The shears in the piers with the lower axial loads were very low and far from their shear strength capacity; vice-versa bending moments were relatively high, confirming the tendency toward flexural collapse. This result agrees with the slenderness of the piers.

The complete set of the most significant results is summarized in Table 6, Table 7 and in Fig. 11. In the piers, the flexural failure mode was prevalent, especially in reinforced walls in which ρ_{fx} is over 2.0 (and greater than 1.0 in a significant number of cases). Ratios ρ_{s1}, and ρ_{s2} are lower than 1.0 with few exceptions. The same trend was detected for the spandrels, but in this case the ratios are much higher than those of the piers. Apart from the anomalous case of ρ_{fx} for URS walls, RSB walls showed the highest flexural and shear forces among all masonry walls, even if ratios ρ were greater than 1.0 also in RSC walls. This result suggests that the spandrels can develop inner forces much higher than those predicted by the considered strength models, especially in the reinforced configuration, i.e. with the tie passing through. The cases with $\rho > 1$ are numerous, and neither flexural nor shear collapse mode were prevalent in reinforced walls. The maximum ratios ρ for all the 27 analyzed walls are presented in Fig. 11. As expected, the greater values were detected in the slenderer spandrels (A walls) in flexure.

Overall, while for masonry piers the bending moments were generally higher than the flexural strengths predicted by IBC models but the shear forces were lower, the spandrels were able to develop both flexural and shear strengths much higher than those predicted by the same models. This suggested to analyze the reliability of the IBC strength models considering both the shear deformation and the internal forces.

4.3. *Reliability of the strength models provided by the IBC*

To distinguish the panels that reached the full strength from those that were far from collapse, a simplified criterion was used, based on the measure of the cord rotation γ_2 of Eq. (15). Different limits for γ_2 were fixed for piers and spandrels based on three hypotheses. Those limits were selected taking into account the slenderness of the panels by a proper calibration procedure according to the FE results in terms of diagram $V - \delta$ and considering the damage level. For a pier of slenderness $\lambda = h/b$, these limits were $\gamma_2{}^* = k\,\lambda$ with $k = 0.4$ ‰, 0.5 ‰ and 0.6 ‰, while for a spandrel of slenderness $\lambda = b/h$ the same limits were assumed to be $k = 0.7$ ‰, 0.85 ‰ and 1 ‰. Applying such criterion, it was possible to divide the panels in two groups where at the end of each analysis was $|\gamma_2|_{\max} > \gamma_2{}^*$ (group "×" in which the full strength was reached) or $|\gamma_2|_{\max} \le \gamma_2{}^*$ (group "o" in which the full strength was not reached). A statistic report of the number of panels of the two groups is presented in Table 8 in which data are separate for URS, RSB and RSC walls. It is plan to see that the piers were more damaged in the reinforced walls, given that "×" instances were more than double than "o"; while for spandrels the "×" cases in RSB walls were a few, given the presence of the concrete corbels that assured high stiffness to the masonry beams. Regarding the k value, overall there were 158 piers of type "×" with $k = 0.4$ ‰, which corresponded to about 6 cases for each wall, value that decreased to 70 (2.6 cases for each wall) when $k = 0.5$ ‰. $k = 0.4$ ‰ is the most appropriate value in this context, that accounts for the reaching of the maximum base shear of the walls. Similarly, $k = 0.7$ ‰ in spandrels is the most appropriate (3.6 cases for each wall).

The reliability of the strength models was based on the ratio $\rho_{\max} = \max(\rho_{fx}, \rho_{s1}, \rho_{s2})$, as explained in Table 9. In particular, for a panel of group "×" the strength model was considered unsafe when $\rho_{\max} < 1$ (over unsafe if $\rho_{\max} < 0.5$) while the strength model was safe if $\rho_{\max} \ge 1$ (over safe if $\rho_{\max} > 1.5$). As an example, Fig. 12 and Fig. 13 show the ratios $\rho_{\max}$ for $k = 0.5$ ‰ for piers and $k = 0.85$ ‰ for spandrels.

Considering the full set of results for all the 945 piers, a great difference was found depending on the three different choices of the parameter k (Table 10). With $k = 0.4$‰, 96 panels (over 10%) were unsafe, and this number decreased to 34 (3.6 %) and 12 (1.3 %) with $k = 0.5$ ‰ and 0.6 ‰, respectively. On the other hand, the safe panels were 145 (over 15%) irrespectively of k values. In any case, the number of undamaged piers was very high (since many panels were far away from the damaged zone of the walls). Considering the same data, but separate for the URS, RSB and RSC walls (Table 11), no significant differences were found with respect to the whole set of data for unsafe panels, while a higher percentage of safe panels was recorded for the reinforced walls (64 versus 17). Considering $k = 0.5$ ‰, these results suggest that the IBC strength models for piers are acceptable, in particular the flexural strength model, because

Table 6
Statistic of values of the ratios ρ_{fx}, ρ_{s1}, and ρ_{s2} for piers.

	URS walls			RSB walls			RSC walls		
	ρ_{fx}	ρ_{s1}	ρ_{s2}	ρ_{fx}	ρ_{s1}	ρ_{s2}	ρ_{fx}	ρ_{s1}	ρ_{s2}
max	1.53	0.72	0.86	2.42	0.92	1.02	2.28	0.89	1.05
mean	0.59	0.31	0.33	0.79	0.49	0.52	0.81	0.48	0.51
min	0.21	0.04	0.04	0.15	0.04	0.04	0.16	0.06	0.06
n. cases $\rho > 1$	17	0	0	62	0	3	64	0	2
tot. cases = 315									

Table 7
Statistic of values of the ratios ρ_{fx}, ρ_{s1}, and ρ_{s2} for spandrels.

	URS walls			RSB walls			RSC walls		
	ρ_{fx}	ρ_{s1}	ρ_{s2}	ρ_{fx}	ρ_{s1}	ρ_{s2}	ρ_{fx}	ρ_{s1}	ρ_{s2}
max	5.29	1.46	1.49	4.09	2.49	2.54	2.86	1.44	1.43
mean	1.72	0.83	0.84	1.70	1.39	1.41	1.38	0.99	1.00
min	0.33	0.19	0.19	0.29	0.16	0.16	0.26	0.12	0.13
n. cases $\rho > 1$	148	60	65	172	158	161	164	120	123
tot. cases = 216									

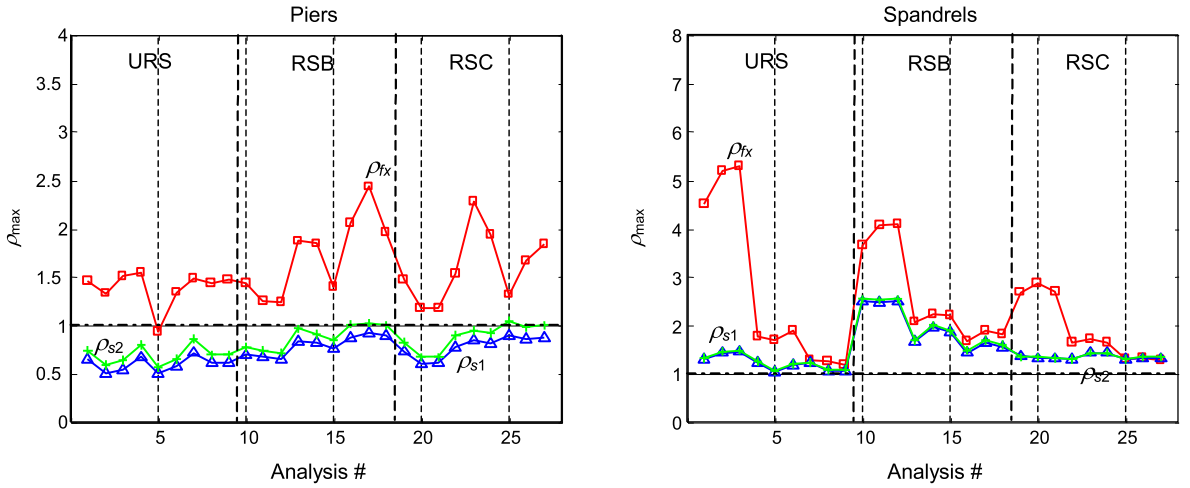

Fig. 11. Maximums ratios ρ_{fx}, ρ_{s1}, and ρ_{s2} for piers and spandrels distinguished for the different walls analysed (red = ρ_{fx}, blu = ρ_{s1}, green = ρ_{s2}).

really many panels collapsed by flexure without developing the full shear strength. However, if $k = 0.4$ ‰ is assumed the percentage of unsafe panels (over 10%) could suggest at least a revision of the M_u formula (Eq. (1)), but the analysis of the ratios ρ revealed values slightly lower than 1.0, showing the acceptability of the flexural model.

For the 648 spandrels, the results were considerably different (Table 10). Only 6 panels (0.9 %) were unsafe with $k = 0.7$ ‰ (number that decreased to 4 and 1 with the increase of k), while 488 panels were safe (over 75 %) regardless of k. This result suggests that the strength models proposed by [36] for spandrels are over-conservative, especially for panels reinforced with a ring beam or by a steel chain (Table 11). A consequence of the low value of the axial force effectively obtained from FE results in masonry beams is that

Table 8
Statistic of number of panels of groups "×" and "o".

	k (‰)	All		USR		RSB		RSC	
		"×"	"o"	"×"	"o"	"×"	"o"	"×"	"o"
Piers	0.4	158	787	31	284	60	255	67	248
	0.5	70	875	12	303	29	286	29	286
	0.6	26	919	4	311	9	306	13	302
Spandrels	0.7	98	550	50	166	5	211	43	173
	0.85	59	589	31	185	4	212	24	192
	1.0	27	621	15	201	4	212	8	208

Table 9
Limits for the ratios ρ_{max} considered to detect the reliability of strength models by IBC.

Ratio ρ_{max}	Panels of group "×"	Panels of group "o"
$\rho_{max} < 0.5$	Over unsafe	Not significant
$0.5 \leq \rho_{max} < 1.0$	Unsafe	Not significant
$1.0 \leq \rho_{max} \leq 1.5$	Safe	Safe
$\rho_{max} > 1.5$	Over safe	Over safe

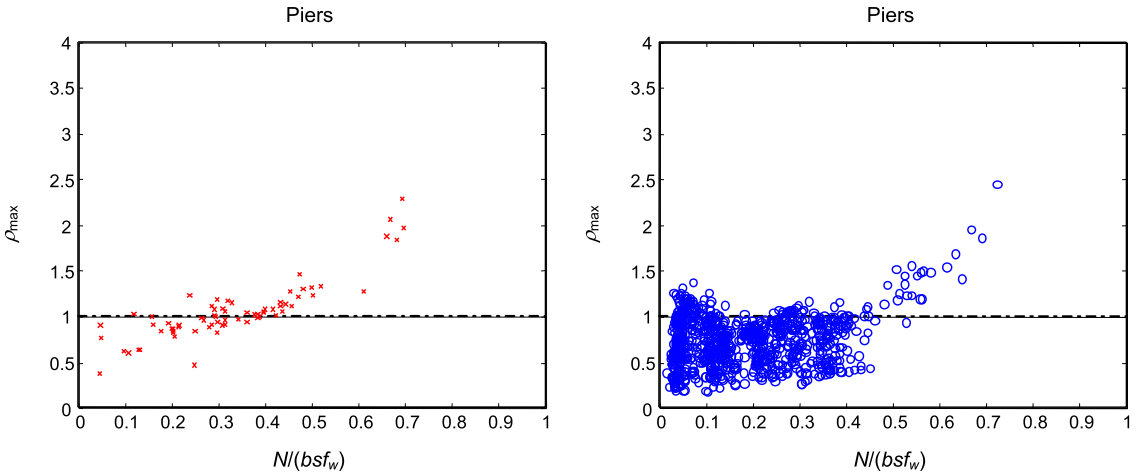

Fig. 12. Ratios ρ_{max} for the whole set of piers distinguished in panels that reached the full strength ("×") and panels that did not reach the full strength ("o"), $k = 0.5$ ‰.

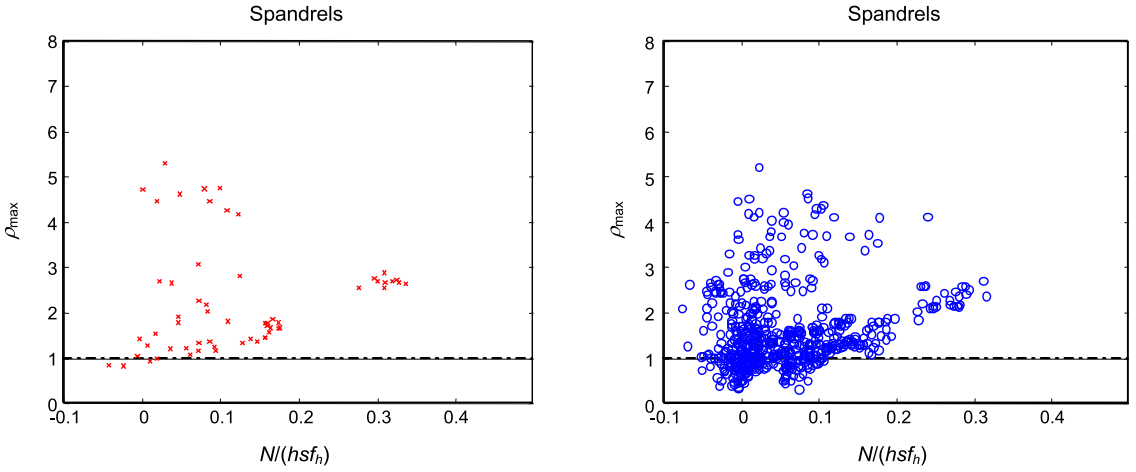

Fig. 13. Ratios ρ_{max} for the whole set of spandrels distinguished in panels that reached the full strength ("×") and panels that did not reach the full strength ("o"), $k = 0.85$ ‰.

the strength models used for piers are either inaccurate or even inapplicable. New models should therefore be investigated. Although the conclusions deriving from the discussed results are strongly dependent on the choice of k, this trend seems clear. In other words, the FE pushover analyses, that allow to correctly simulate the actual boundary conditions of the panels inside the walls, suggested that further studies and investigations are required for spandrels, whereas strength models for piers are reliable.

5. Concluding remarks

To provide an insight on the reliability of the formulae provided by the IBC (similar to the ones reported in the EC) for the flexural and shear strength of masonry piers and spandrels, this paper analyzed the results of 27 pushover analyses performed on 9 different plane brick masonry walls. The considered walls differ in the span-to-height ratio b/h of the masonry beams and in the type of

Table 10
Statistic of values of the ratios ρ_{max} for piers and spandrels.

	k (‰)	All walls				
		(ous)	(us)	(ns)	(s)	(os)
Piers (945)	0.4	2	94	704	133	12
	0.5	2	32	766	133	12
	0.6	1	11	788	133	12
Spandrels (648)	0.7	0	6	154	221	267
	0.85	0	4	156	221	267
	1.0	0	1	159	221	267

(ous) = overunsafe; (us) = unsafe; (ns) = not significant; (s) = safe; (os) = oversafe, $\gamma_2^* = k\ \lambda$.

Table 11
Statistic of values of the ratios ρ_{max} for piers and spandrels for different types of reinforcement.

	k (‰)	URS walls					RSB walls					RSC walls				
		(ous)	(us)	(ns)	(s)	(os)	(ous)	(us)	(ns)	(s)	(os)	(ous)	(us)	(ns)	(s)	(os)
Piers	0.4	2	24	272	15	2	0	32	219	59	5	0	38	213	59	5
	0.5	2	8	288	15	2	0	10	241	59	5	0	14	237	59	5
	0.6	1	3	294	15	2	0	0	251	59	5	0	8	243	59	5
Spandrels	0.7	0	6	61	74	75	0	0	44	53	119	0	0	49	94	73
	0.85	0	4	63	74	75	0	0	44	53	119	0	0	49	94	73
	1.0	0	1	66	74	75	0	0	44	53	119	0	0	49	94	73

(ous) = overunsafe; (us) = unsafe; (ns) = not significant; (s) = safe; (os) = oversafe, $\gamma_2^* = k\ \lambda$.

reinforcement used. The FE method with a smeared crack approach was employed to reproduce the masonry nonlinear behavior. The numerical analyses, considering a whole masonry façade, have the advantage to accurately represent the current distribution of the inner forces in the masonry piers and spandrels during the loading process, thus appropriately simulating the boundary conditions of the masonry panels. Results of the analyses led to the following remarks.

The evolutions of the cracking patterns in the masonry panels did not display in most cases a clear collapse mode, i.e. shear by diagonal cracking or flexural mode. The uncertainties about the boundary conditions of a masonry pier or spandrel in the wall, and their evolution during the loading process, were the main reason that accounted for this result. Nonetheless, to investigate the reliability of the IBC strength models, a criterion based on a global deformability index was here adopted. This criterion, although approximate, was able to identify a general trend and to discern the type of failure in masonry beams.

The analysis of the results showed that the strength models provided by IBC for the masonry piers that prevalently collapsed by bending are reliable. The ratios between the bending moments obtained by the FE analyses and those predicted by the strength bending models were greater than 1.0, or they were slightly lower than 1.0. On the contrary, the strength models for spandrels were found to be inadequate, given that the shear forces obtained by FE analyses were significantly higher than those predicted by the IBC strength models. This means that the strength models provided by the Standards largely underestimate the real strength both in unreinforced and strengthened walls, especially in the case of slender spandrels in the strengthened walls. This result was more evident in the RSB walls (the ones strengthened with a concrete ring beam). In view of this, the results here discussed suggest that further numerical and experimental studies should be performed to investigate reliable formulae for assessing the failure strength of masonry spandrels.

Declaration of Competing Interest

The authors declare that they have no known competing financial interests or personal relationships that could have appeared to influence the work reported in this paper.

Data availability

Data will be made available on request.

Acknowledgments

The author F.J. Pallarés would like to express his sincere gratitude to the Generalitat Valenciana for supporting and financing through the CIBEST/2021/235 Grant a research stay at the University of Florence.

References

[1] G. Vlachakis, E. Vlachaki, P.B. Lourenço, Learning from failure: Damage and failure of masonry structures, after the 2017 Lesvos earthquake (Greece), Eng. Fail. Anal. 117 (2020), 104803, https://doi.org/10.1016/j.engfailanal.2020.104803.

[2] G. Lucibello, G. Brandonisio, E. Mele, A. De Luca, Seismic damage and performance of Palazzo Centi after L'Aquila earthquake: a paradigmatic case study of effectiveness of mechanical steel ties, Eng. Fail. Anal. 34 (2013) 407–430, https://doi.org/10.1016/j.engfailanal.2013.09.011.
[3] V. Cardinali, M. Tanganelli, R. Bento, Seismic assessment of the XX century masonry buildings in Florence: Vulnerability insights based on urban data acquisition and nonlinear static analysis, Journal of Building Engineering 57 (2022), 104801, https://doi.org/10.1016/j.jobe.2022.104801.
[4] P. Foraboschi, Coupling effect between masonry spandrels and piers, Mater. Struct. 42 (2009) 279–300, https://doi.org/10.1617/s11527-008-9405-7.
[5] H. Pirsaheb, P. Wang, M.J. Moradi, G. Milani, A Multi-Pier-Macro MPM method for the progressive failure analysis of perforated masonry walls in-plane loaded, Eng. Fail. Anal. 127 (2021) (2021), 105528, https://doi.org/10.1016/j.engfailanal.2021.105528.
[6] M. Betti, L. Galano, A. Vignoli, Comparative analysis on the seismic behaviour of unreinforced masonry buildings with flexible diaphragms, Eng. Struct. 61 (2014) 195–208, https://doi.org/10.1016/j.engstruct.2013.12.03.
[7] M. Valente, G. Milani, Damage assessment and collapse investigation of three historical masonry palaces under seismic actions, Eng. Fail. Anal. 98 (2019) 10–37, https://doi.org/10.1016/j.engfailanal.2019.01.066.
[8] F. Clementi, G. Milani, A. Ferrante, M. Valente, S. Lenci, Crumbling of Amatrice clock tower during 2016 Central Italy seismic sequence: Advanced numerical insights, Frattura ed Integrità Strutturale 51 (2020) 313–335, https://doi.org/10.3221/IGF-ESIS.51.24.
[9] M. Valente, Seismic behavior and damage assessment of two historical fortified masonry palaces with corner towers, Eng. Fail. Anal. 134 (2022), 106003, https://doi.org/10.1016/j.engfailanal.2021.106003.
[10] Y.T. Guo, D.V. Bompa, A.Y. Elghazouli, Nonlinear numerical assessments for the in-plane response of historic masonry walls, Eng. Struct. 268 (2022), 114734, https://doi.org/10.1016/j.engstruct.2022.114734.
[11] F. Parisi, G.P. Lignola, N. Augenti, A. Prota, G. Manfredi, Rocking response assessment of in-plane laterally-loaded masonry walls with openings, Eng. Struct. 56 (2013) 1234–1248, https://doi.org/10.1016/j.engstruct.2013.06.041.
[12] T. Choudhury, G. Milani, H.B. Kaushik, Experimental and numerical analyses of unreinforced masonry wall components and building, Constr. Build. Mater. 257 (2020), 119599, https://doi.org/10.1016/j.conbuildmat.2020.119599.
[13] K.A.S. Medeiros, G.A. Parsekian, N.G. Shrive, F.S. Fonseca, Shear load capacity prediction of unperforated and perforated partially grouted masonry walls, Eng. Struct. 256 (2022), 113927, https://doi.org/10.1016/j.engstruct.2022.113927.
[14] A. Brencich, L. Gambarotta, S. Lagomarsino, A macro-element approach to the three-dimensional seismic analysis of masonry buildings, in: Proc. 11th European Conference on Earthquake Engineering, Paris, France (1998).
[15] S. Lagomarsino, A. Penna, A. Galasco, S. Cattari, TREMURI program: an equivalent frame model for the nonlinear seismic analysis of masonry buildings, Eng. Struct. 56 (2013) 1787–1799, https://doi.org/10.1016/j.engstruct.2013.08.002.
[16] G. Longobardi, A. Formisano, Seismic vulnerability assessment and consolidation techniques of ancient masonry buildings: The case study of a Neapolitan Masseria, Eng. Fail. Anal. 138 (2022), 106306, https://doi.org/10.1016/j.engfailanal.2022.106306.
[17] C. Morandini, D. Malomo, A. Penna, Equivalent frame discretisation for URM façades with irregular opening layouts, Bull. Earthq. Eng. 20 (2022) 2589–2618, https://doi.org/10.1007/s10518-022-01315-0.
[18] M. Tomazevic, V. Turnsek, S. Tertelj, Computation of the Shear Resistance of Masonry Buildings. Report ZRMK-ZK, Institute for Testing and Research in Materials and Structures, Ljubljana (in Slovenian) (1978).
[19] M. Tomazevic, The computer program POR. Report ZRMK, Institute for Testing and Research in Materials and Structures, Ljubljana (in Slovenian) (1978).
[20] G. Magenes, S. Della Fontana, Simplified Non-linear Seismic Analysis of Masonry Buildings, Proc. Brit. Masonry Soc. 8 (1998) 190–195.
[21] R. Marques, P.B. Lourenço, Possibilities and comparison of structural component models for the seismic assessment of modern unreinforced masonry buildings, Comput. Struct. 89 (21–22) (2011) 2079–2091, https://doi.org/10.1016/j.compstruc.2011.05.021.
[22] E. Quagliarini, G. Maracchini, F. Clementi, Uses and limits of the Equivalent Frame Model on existing unreinforced masonry buildings for assessing their seismic risk: A review, J. Build. Eng. 10 (2017) 166–182, https://doi.org/10.1016/j.jobe.2017.03.004.
[23] G. Magenes, G.M. Calvi, In-plane seismic response of brick masonry walls, Earthq. Eng. Struct. Dyn. 26 (1997) 1091–1112, https://doi.org/10.1002/(SICI)1096-9845(199711)26:11<1091::AID-EQE693>3.0.CO;2-6.
[24] C. Calderini, S. Cattari, S. Lagomarsino, In-plane strength of unreinforced masonry piers, Earthq. Eng. Struct. Dyn. 38 (2) (2009) 243–267, https://doi.org/10.1002/eqe.860.
[25] M. Betti, L. Galano, M. Petracchi, A. Vignoli, Diagonal cracking shear strength of unreinforced masonry panels: a correction proposal of the *b* shape factor, Bull. Earthq. Eng. 13 (10) (2015) 3151–3186, https://doi.org/10.1007/s10518-015-9756-8.
[26] K. Beyer, S. Mangalathu, Review of strength models for masonry spandrels, Bull. Earthq. Eng. 11 (2013) 521–542, https://doi.org/10.1007/s10518-012-9394-3.
[27] M. Betti, L. Galano, A. Vignoli, Seismic Response Of Masonry Plane Walls: A Numerical Study On Spandrel Strength, AIP Conf. Proc. 1020 (2008) 787–794, https://doi.org/10.1063/1.2963915.
[28] H. Tariq, M.A. Najafgholipour, V. Sarhosis, G. Milani, In-plane strength of masonry wall panels: A comparison between design codes and high-fidelity models, Structures 47 (2023) 1869–1899, https://doi.org/10.1016/j.istruc.2022.11.125.
[29] G. Rinaldin, C. Amadio, N. Gattesco, Review of experimental cyclic tests on unreinforced and strengthened masonry spandrels and numerical modelling of their cyclic behaviour, Eng. Struct. 132 (2017) 609–623, https://doi.org/10.1016/j.engstruct.2016.11.063.
[30] K. Beyer, A. Dazio, Quasi-Static Monotonic and Cyclic Tests on Composite Spandrels, Earthq. Spectra 28 (3) (2012) 885–906, https://doi.org/10.1193/1.4000058.
[31] K. Beyer, Peak and residual strengths of brick masonry spandrels, Eng. Struct. 41 (2012) 533–547, https://doi.org/10.1016/j.engstruct.2012.03.015.
[32] F. Parisi, N. Augenti, Seismic capacity of irregular unreinforced masonry walls with openings, Earthq. Eng. Struct. Dyn. 42 (2013) 101–121, https://doi.org/10.1002/eqe.2195.
[33] A. Sandoli, C. Musella, G.P. Lignola, B. Calderoni, A. Prota, Spandrel panels in masonry buildings: Effectiveness of the diagonal strut model within the equivalent frame model, Structures 27 (2020) 879–893, https://doi.org/10.1016/j.istruc.2020.07.001.
[34] A. Sandoli, B. Calderoni, G.P. Lignola, A. Prota, Effect of the axial force on shear and flexural strength of masonry spandrels, Bull. Earthq. Eng. 21 (5) (2023) 2947–2985, https://doi.org/10.1007/s10518-023-01637-7.
[35] M. Berti, L. Salvatori, M. Orlando, P. Spinelli, Unreinforced masonry walls with irregular opening layouts: reliability of equivalent-frame modelling for seismic vulnerability assessment, Bull. Earthq. Eng. 15 (2017) 1213–1239, https://doi.org/10.1007/s10518-016-9985-5.
[36] MIT. D.M. del Ministero delle Infrastrutture e dei Trasporti del 17/01/2018. Aggiornamento delle Norme Tecniche per le Costruzioni (NTC 2018). G.U. n. 42 del 20.02.2018. S.O. n. 8. (in Italian) (2018).
[37] MIT. Circolare n. 7 del 21 gennaio 2019 del Ministero delle Infrastrutture e dei Trasporti. Istruzioni per l'applicazione dell'Aggiornamento delle "Norme tecniche per le costruzioni" di cui al Decreto Ministeriale 17 gennaio 2018. (in Italian) (2019).
[38] V. Turnšek, F. Cacovic, Some experimental results on the strength of brick masonry walls, in: Proc. 2nd International Brick Masonry Conference, Stoke on Trent, United Kingdom, (1970) 149–156.
[39] M. Betti, L. Galano, Shear strength of rubble stone-and-brick masonry panels. A new proposal for the interpretation of Sheppard test results, Constr. Build. Mater. 279 (2021), 121925, https://doi.org/10.1016/j.conbuildmat.2020.121925.
[40] M. Krzan, S. Gostic, S. Cattari, V. Bosiljkov, Acquiring reference parameters of masonry for the structural performance analysis of historical buildings, Bull. Earthq. Eng. 13 (2015) 203–236, https://doi.org/10.1007/s10518-014-9686-x.
[41] S. Boschi, L. Galano, A. Vignoli, Mechanical characterisation of Tuscany masonry typologies by in situ tests, Bull. Earthq. Eng. 17 (1) (2019) 413–438, https://doi.org/10.1007/s10518-018-0451-4.
[42] ANSYS. ANSYS Manual v. 11.0. Set: ANSYS Inc., Canonsburg, PA, USA, (1998).

[43] D.C. Drucker, W. Prager, Soil mechanics and plastic analysis or limit design, Q. Appl. Math. 10 (2) (1952) 157–165. https://www.jstor.org/stable/43633942.
[44] K.J. Willam, E.D. Warnke, Constitutive Model for the Triaxial Behavior of Concrete, in: Proc. International Association for Bridge and Structural Engineering, 19, ISMES, Bergamo, Italy (1975).
[45] M. Betti, L. Galano, A. Vignoli, Finite element modelling for seismic assessment of historic masonry buildings, in: S. D'Amico (ed), Earthquakes and Their Impact on Society. Springer Natural Hazards, (2016) 377–415. https://doi.org/10.1007/978-3-319-21753-6_14.